Stresses Induced in Iron-Ore Pellets by Hydrogen Reduction

MARC ANDRÉ MEYERS and TAVEESIRI TANTEVEE

The objectives of this investigation were (a) to determine the effect of reduction temperature on the strength of iron ore agglomerates and (b) to develop enhanced understanding for the cracking associated with reduction. Iron-ore agglomerates from two sources (Samarco Mineração and Bethlehem Steel) were reduced in a hydrogen atmosphere at temperatures varying from 873 K to 1373 K at intervals of 100 K and times varying from 30 to 300 minutes. The compressive strength at the ambient temperature of the pellets was determined after the various reduction treatments by using a piston-and-cylinder testing technique and computing the energy required in crushing them. The highest strength, at a specific level of reduction, was found after reduction at 1073 K, for both the Samarco and Bethlehem pellets. Profuse cracking of the pellets was observed after reduction. These cracks led to a weakening of the pellets. A mechanism for reduction-induced cracking, based on internal stresses due to volume changes produced by the chemical reactions, is presented.

I. INTRODUCTION

THE reduction of iron oxides by gases is a thoroughly studied phenomenon[1] that has found a wide technological application.[2] However, many poorly understood factors still exist, such as the effect of pellet composition and reducing gas on dimensional changes during reduction.[3] These dimensional changes are of great importance, and Meyer[4] attributes the loss in strength during reduction in part to swelling associated with phase transformations. Taniguchi and Ohmi[5,6] and Taniguchi *et al.*[7] have shown that the loss in strength of iron-ore pellets reduced in hydrogen is closely related to the degree of maximum swelling. They observed cracking on the surfaces of the reduced pellets. The pellets reduced at temperatures where maximum cracking was observed exhibited the least crushing strength, leading Taniguchi and Ohmi[5,6] to attribute the low strength to stress concentrations at the crack tips. In spite of the qualitative statements by Meyer[4] and Taniguchi and Ohmi,[5,6] no quantitative analyses of the stresses involved have yet been performed. The determination of the loss of strength after reduction, the observation of reduction-induced cracking, and the establishment of the mechanism(s) responsible constituted the primary goals of the investigation whose results are described herein. It should be emphasized that reduction by hydrogen is not a standard industrial practice; most direct reduction plants utilize CO/CO_2 or $H_2/CO/CO_2$ mixtures as reducing gases. For CO/CO_2 mixtures, the topochemical reaction is not observed.

II. EXPERIMENTAL PROCEDURES

A. *Materials*

The investigation was carried out using hematite and magnetite pellets which were kindly supplied by the Samarco Mineração and Bethlehem Steel Corporation, respectively. It should be specified that the Bethlehem pellets are transformed to hematite during the sintering process and are, as a result, fully hematitic, in spite of the fact that they originate from taconite (magnetite) deposits. The iron, silicon, and calcium weight percents were analyzed to be 66.60, 2.44, 1.45 for the Samarco pellets and 67.89, 2.38, 0.26 for the Bethlehem pellets. The porosities and apparent densities were 22 pct, and 4.0 g/cm^3 for the Samarco pellets and 23 pct and 3.9 g/cm^3 for the Bethlehem pellets.

Bethlehem pellets had optimum roundness and quite a smooth surface in the as-received condition, but Samarco pellets needed to be ground down for optimum roundness and a smooth surface. Uniform size and shape of pellets was produced by grinding in a ball mill for 36 hours and using a vibratory screening machine. After screening, the pellet diameters for both ranged from 9.52 to 12.70 mm. Pure hydrogen (99.99 pct min.) was used as the reducing gas.

B. *Reducing Apparatus and Procedure*

The experimental reducing apparatus is shown in Figure 1. This investigation used a horizontal tube furnace with an alumina tube. It was equipped with a stainless steel cylindrical rotary sample holder with 5 mm holes on the lateral walls and ends. The cylindrical sample holder (M) had a length of 400 mm and diameter of 40 mm. Along its axis two stainless steel shafts assured the positioning of the sample holder. They were positioned by two stainless steel stoppers (K), which contained pressure-fit and gas-tight O-ring seals. The rotary sample holder was manually rotated every 3 minutes to assure an even flow of hydrogen to the pellets. A lot of 20 pellets was placed in the rotary sample holder. The rotary sample holder was introduced into the middle of the reduction furnace having the uniform temperature zone adjacent to a thermocouple. Flow of nitrogen gas was commenced through a flowmeter and a stainless steel tube (F), which was maintained at about 873 K by another electric furnace (E). This removed any oxygen present in the nitrogen. After removal of oxygen, the gas was passed through two drying bottles containing anhydrous calcium sulfate (G) where water vapor was removed; finally, pure nitrogen gas was passed through the refractory tube containing the sample holder. Once the pellets under nitrogen atmosphere attained a desired temperature, the flow of

MARC ANDRÉ MEYERS is Associate Director, Center for Explosives Technology Research, New Mexico Institute of Mining and Technology, Socorro, NM 87801. TAVEESIRI TANTEVEE, formerly Graduate Student, Department of Metallurgical and Materials Engineering, New Mexico Institute of Mining and Technology, is with the Office of Basic Industry Development, Bangkok, Thailand.

Manuscript submitted April 8, 1985.

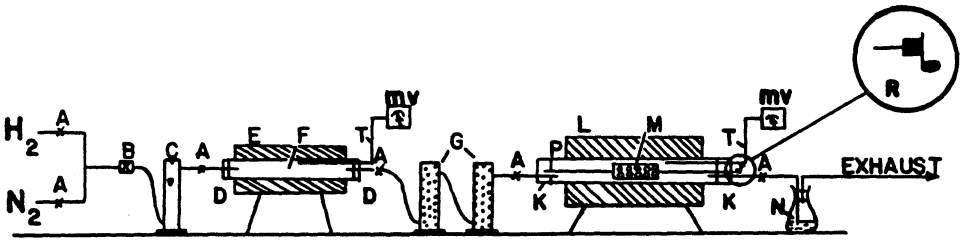

A Needle Valves	B Check valves
C Flowmeter	D Rubber stoppers
E Electric Furnace	F Stainless steel tube
G Drying Bottles	K Stainless steel stoppers
L Electric Furnace	N Rotary sample holder
N Absorption Flasks	P Refractory tube
T Thermocouples	R Manual Crank

Fig. 1—Schematic representation of experimental reduction apparatus.

nitrogen was discontinued; immediately thereafter, hydrogen flow was commenced. Sufficient time (about 3 minutes) was allowed for the hydrogen gas to replace the nitrogen remaining in the drying bottles. Care was taken, particularly during the early stages of reduction, to hold the rate of the hydrogen flow at 400 cm^3 per minute. At the desired time the hydrogen flow was stopped and the nitrogen flow was started again. The reduced pellets were then allowed to cool in the nitrogen atmosphere. The water formed during reduction was collected in a 250 cm^3 Erlenmeyer flask (N) containing 100 cm^3 of concentrated H_2SO_4. Renewal of the acid, after about 30 minutes reduction time, assured satisfactory absorption of the water. The absorption flask was placed close to the outlet of the reduction furnace to prevent condensation of water vapor formed. The pellets and flask were weighed before and after the reduction test. The actual weight loss of pellets was determined. The amount of water formed was weighed at 30-minute intervals. Percent reduction was determined by the weight loss of the pellets. The theoretical weight loss was calculated by assuming that all iron in pellets was in the form Fe_2O_3 and oxygen was completely removed.

C. *Metallographic Examination*

Scanning electron microscopy together with energy dispersive X-ray spectrometry was performed using a Hitachi-Perkin Elmer Model HHS-2R scanning electron microscope; both the surface and the interior of the pellets were analyzed. In addition, optical micrographs and macrographs were also taken of selected cross-sections of the pellets. The pellets were mounted by using the Epo-Kwick epoxy mounting system; no heating or pressure was required, ensuring the fact that no cracks were introduced during preparation. The mounted pellets were sectioned by an abrasive cutter using a 1.8 mm thick cut-off wheel.

D. *Mechanical Testing*

The compressive strength of the pellets was determined at ambient temperature in a Tinius-Olson testing machine using a piston-and-cylinder testing technique. This testing procedure, which was developed by Meyers and Meyers,[8] uses a thick-walled cylinder and a loosely fitting piston. One of the major problems in determining the compressive strength of pellets according to the established practice[9] (compressing one pellet between two parallel plates until fracture occurs) is the great degree of variation between tests, requiring large number of tests to obtain statistically significant results. Meyers and Meyers[4] proposed a simple alternative, consisting of a thick-walled cylinder in which a piston penetrates. A large group of pellets can be tested simultaneously, and one single test is sufficient to characterize the mechanical response of the pellets. The system used by Meyers and Meyers[8] accommodated over two hundred pellets. A smaller one was built for the specific needs of this investigation. A sketch of the setup is shown in Figure 2. The piston-and-cylinder setup is placed between two parallel plates and compressed in a mechanical testing machine that has the appropriate load and displacement recording capability. The height of the system was 150 mm and internal diameter was 27 mm. The system was compressed at a velocity of 1.3 mm/min which provided a strain rate of $4. \times 10^{-4}\ s^{-1}$. The piston movement was obtained from the cross-head and recorder velocities. Fifteen pellets were loaded into the cylinder. Before and after crushing, the height of pellets was measured. The energies required to crush the pellets to an arbitrarily chosen strain of 0.3 were found out by measuring the area under the load *vs* displacement curve.

Hence, these numbers represent the energy expended in the crushing of fifteen pellets. One would obtain a normalized energy dividing these numbers by the volume or by the

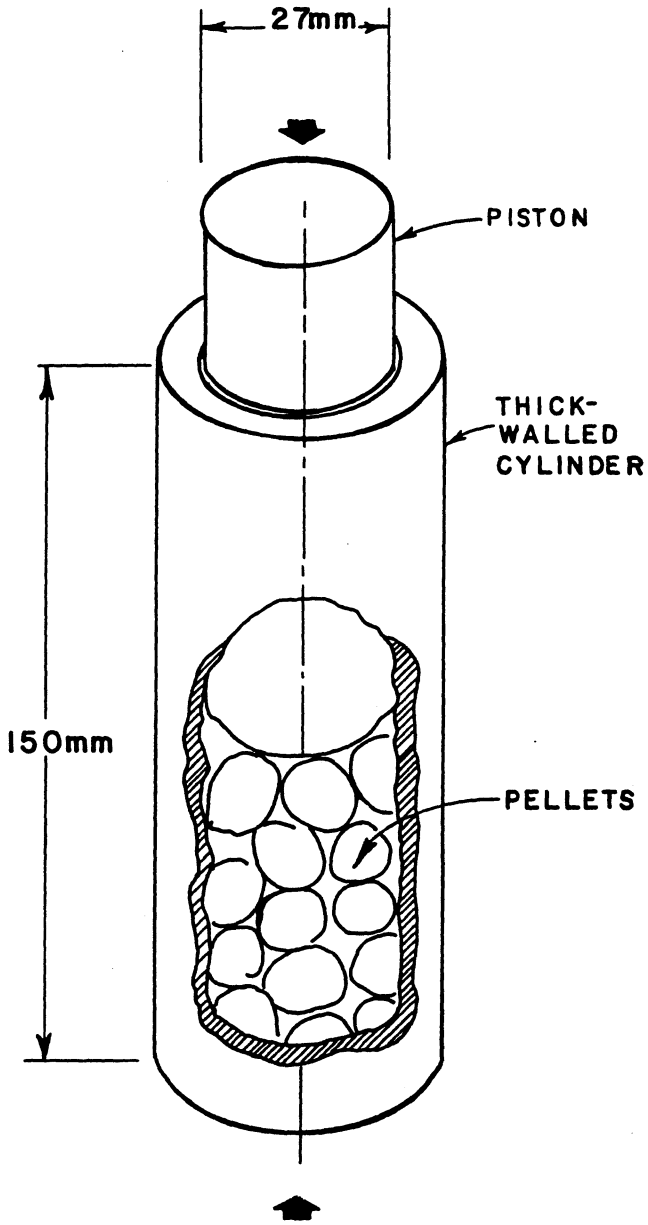

Fig. 2 — Sketch of piston-and-cylinder setup used to determine mechanical strength of pellets.

number of pellets. The stress was calculated by dividing the load by the cross-sectional area of the piston; the strain was obtained by dividing the displacement by the initial height of the pellet stack.

III. EXPERIMENTAL RESULTS

No attempt was made in this investigation to determine the kinetic parameters governing the reduction reaction. This has been done thoroughly in a number of prior investigations.[1,10-15] The reduction experiments were conducted with the objectives of (a) observing the cracks generated in the reduced pellets and (b) determining the mechanical strength of the reduced pellets. Reduction experiments were conducted at temperatures of 873, 973, 1073, 1173, 1273, and 1373 K and time increments of 30 mn (up to 5 hours) at each temperature. Separate reduction experiments were conducted for Samarco and Bethlehem Steel pellets.

The macroscopic examination of the cross-section of some reduced pellets for various reduction treatments indicated that the amount of reduction in all the pellets for each reduction treatment was reasonably consistent. Differences in the thicknesses of the reduced layers could be observed, and alterations in the shape of the interfaces due to cracking were present, but no drastic inconsistences were observed.

Surface and cross-sectional features of pellets reduced for two hours at various temperatures are shown in Figure 1. For most cases profuse cracking was associated with reduction. The possible causes for cracking are discussed in Section IV. As stated above, this investigation did not have as its objective the analysis of the reduced layers and reduction kinetics. Hence, no detailed discussion will be given on the different layers observed and visible in Figure 3. One can say that a topochemical pattern was developed during reduction.

The macrographic examination of some reduced pellets indicated that most of the cracks were actually formed during the reduction of the pellets and not during the heating or cooling process as can be seen in Figure 4. This is evident from the fact that the lighter region on the cross-section of the pellets is distorted away from the cracks; since this lighter region forms during the reduction process and cracking precedes the distortion of the interface, one can conclude that the cracks also form during the reduction process and not during the actual cooling down.

In addition to the cracks observable by the naked eye, scanning electron microscopy revealed microcracks at the surface of the reduced pellets. Figure 5 shows a microcrack in a Samarco pellet reduced at 1273 K to a 91 pct reduction. At lower magnification (Figure 3(a)) it is barely visible (arrow); however, at higher magnification two cracks can be seen.

The load *vs* displacement curves using the piston-and-cylinder testing method for fifteen Bethlehem pellets prior to reduction (two different tests) are shown in Figure 6(a). The curves appear somewhat irregular. As the piston descends, the pellets get crushed; the rupture of pellets is indicated by sudden drops in the load *vs* displacement curve. As the cracks develop on rupture, the pellets become better packed and can sustain more load so that a progressively higher load is required which results in the upwardly concave load *vs* displacement curve. After full densification, the curve should asymptotically approach the elastic loading line for the ore. Since fifteen pellets are involved, the individual fracture events average out, resulting in a somewhat smooth transformed stress-strain curve. Meyers and Meyers[8] used over two hundred pellets per test and obtained, as a result, much smoother curves. Nevertheless, it is felt that fifteen pellets are enough to characterize the mechanical strength, and the results are satisfactory. After reduction the curves become much smoother due to the production of more ductile constituents. The schematic representation of stress *vs* strain curves for three different conditions (one prior to reduction and two after reduction) is shown in Figure 6(a). It can be clearly seen that reduction has a marked effect on strength.

The energy required in the crushing process *vs* percent reduction at each reduction temperature for Samarco and Bethlehem pellets is shown in Figures 7(a) and 7(b). The

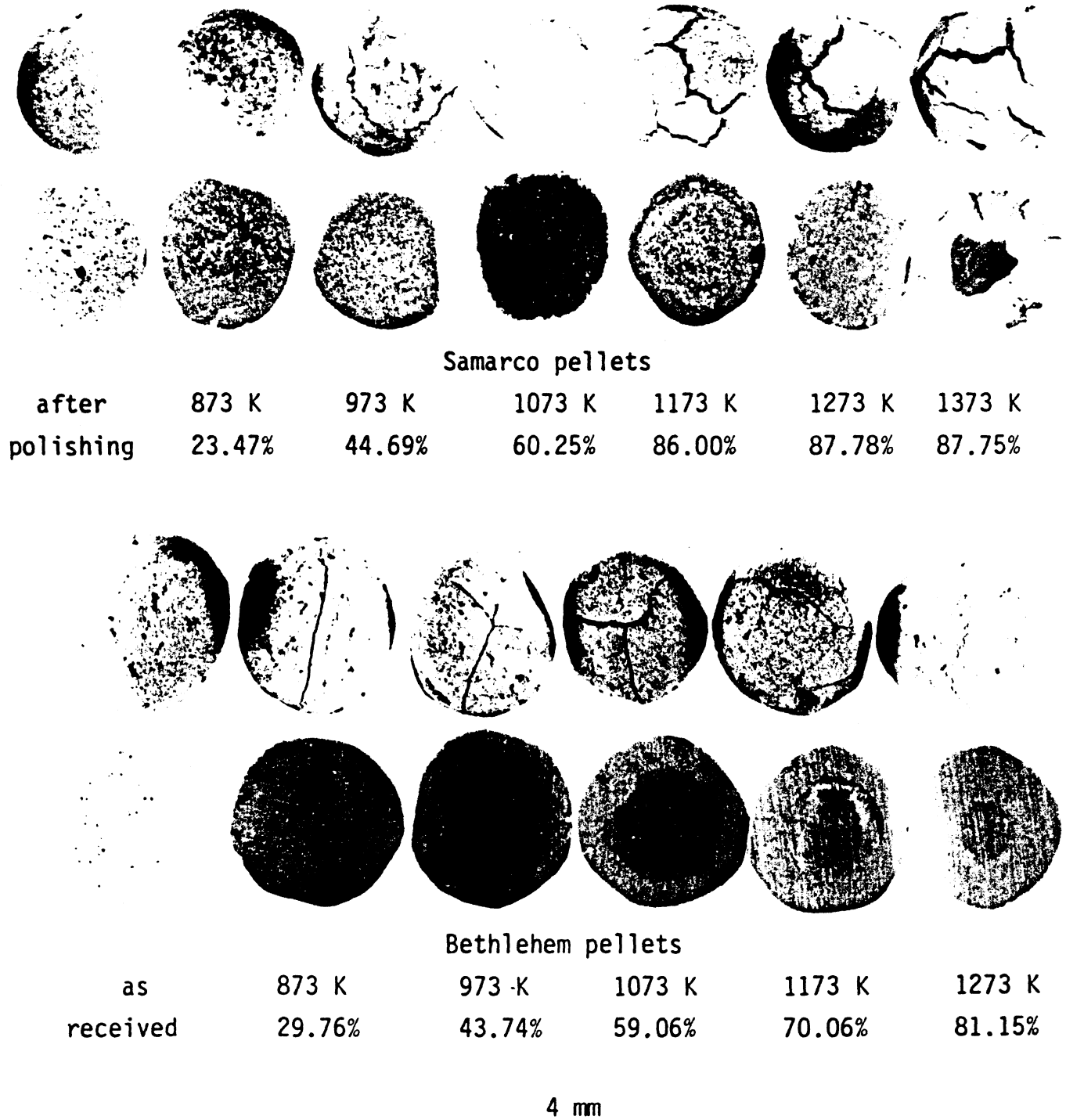

Fig. 3 — Surface and cross-section features of pellets reduced for two hours at various temperatures. Reduction temperature and percentage indicated below each condition. Samarco pellets were polished in ball mill to improve roundness.

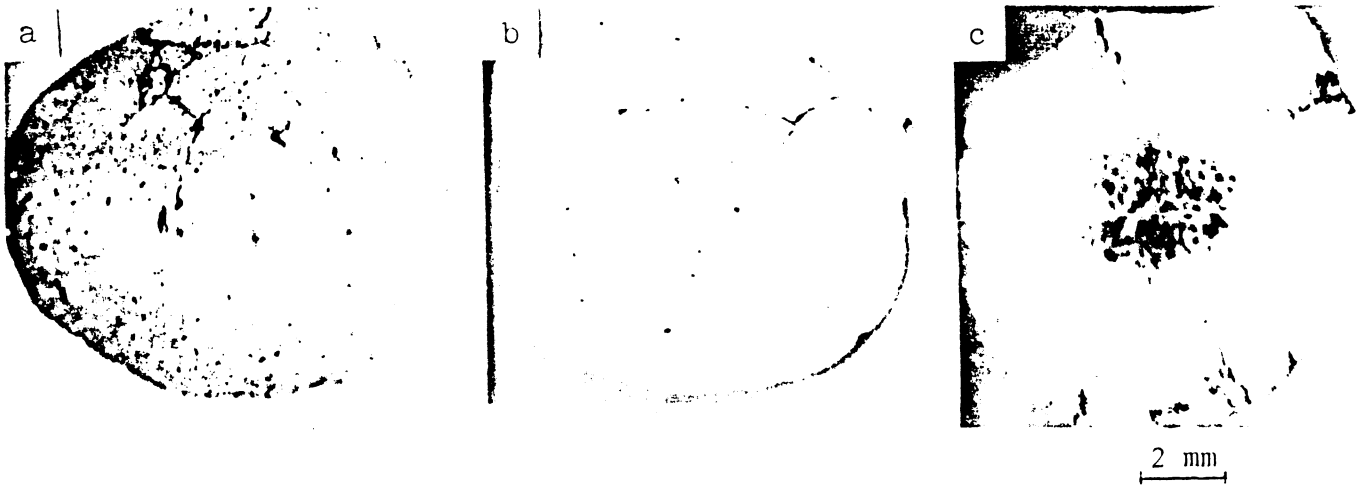

Fig. 4—Cross-section of reduced pellets showing sharp interface away from cracks. (*a*) Samarco pellet, 1173 K, 96 pct, 150 min. (*b*) Bethlehem pellet, 1073 K, 97 pct, 240 min. (*c*) Samarco pellet, 1173 K, 75 pct, 90 min.

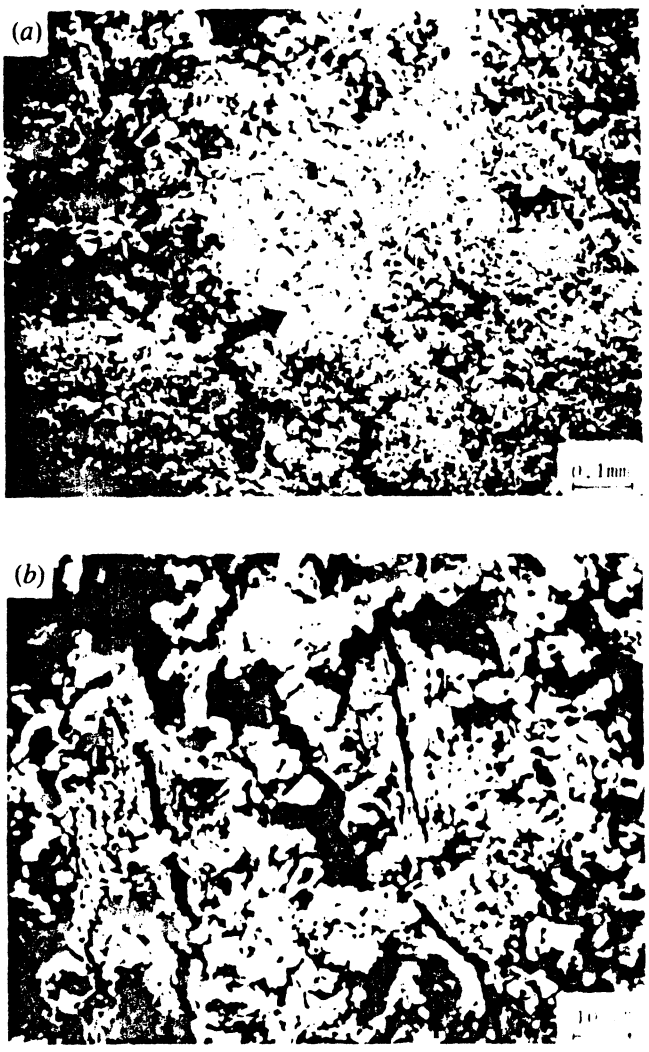

Fig. 5—Microcracks at surface of Samarco pellet reduced at 1273 K to a 91 pct reduction: (*a*) microcrack marked with arrow, (*b*) higher magnification of microcrack.

strength prior to reduction of Samarco pellets (120 N.m) was found to be higher than that of Bethlehem pellets (80 N.m). This is due to two reasons. First, Hoffman *et al.*[16] found that CaO additions increased the strength of fired iron-ore pellets; the Samarco pellets have a substantially higher CaO content (1.45 pct) than the Bethlehem Steel ones (0.26 pct). Furthermore, the strength of Samarco pellets (made from hematite concentrates) is achieved through recrystallization and grain growth during induration, in contrast to the Bethlehem Steel pellets (made from magnetite concentrates) where oxidation also occurs; this is discussed by Meyer.[17]

For all cases, reduction decreased the strength of the pellets. The first 20 pct reduction seems to produce the most drastic changes. There do not seem to be any major differences between the loss of strength of Samarco and Bethlehem Steel pellets due to reduction. At a same degree of reduction, the pellets reduced at 1073 K exhibit the highest strength. This agrees with Taniguchi and Ohmi,[5] who found the highest strength after reducing the pellets at 1023 K (in hydrogen atmosphere).

IV. STRESS ANALYSIS OF PELLETS DURING REDUCTION

As discussed in the preceding section, cracks were observed after reduction. There are several possible reasons for cracking; no clarifying information could be found in the literature. The three most likely reasons are: (a) volume changes due to transformations from one phase to another, (b) pressure in internal pores caused by hydrogen dissolved at reduction temperature diffusing out as the pellets are cooled, and (c) thermal stresses on heating and cooling.

Figure 8 shows typical cracks observed in the reduced pellets. These cracks can be divided into two classes: radial cracks, shown in Figure 8(a), and circumferential cracks, shown in Figure 8(b).

The pressure of dissolved hydrogen induced by cooling down in the pellets is calculated in Section IV-A. The stresses induced by the transformation volume changes of the pellets are calculated in Section IV-B. The hypothesis of

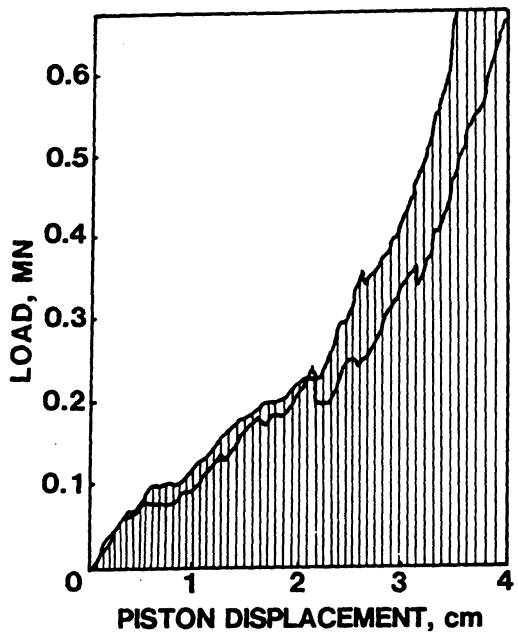

(a)

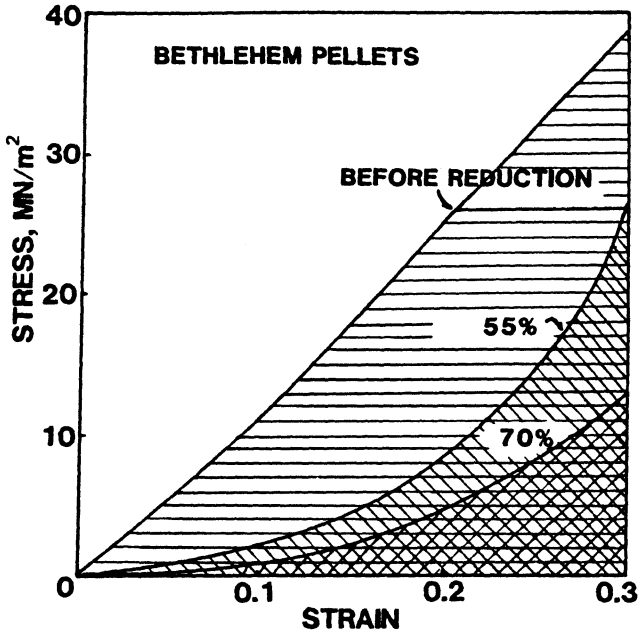

(b)

Fig. 6—(*a*) Load *vs* displacement curves using piston-and-cylinder testing method for fifteen Bethlehem pellets prior to reduction (two different tests). (*b*) Schematic representation of stress *vs* strain curves for Bethlehem pellets reduced at 1173 K; before reduction, 55 pct and 70 pct reduction as strong, medium, and weak pellets, respectively.

thermal stresses was discarded when a pellet was heated up to reduction temperature and maintained at that temperature for two hours and subsequently cooled down to room temperature in the absence of reduction, as no cracks were observed.

A. *Pressure Induced by Trapped Hydrogen*

The calculation was conducted for one completely reduced pellet with original diameter of 1.11 cm, porosity of 22 pct, and Fe_2O_3 density of 6.849 g/cm^3. The solubility of hydrogen at 1 atm pressure in iron is 0.0625 cm^3 per gram of iron.[18] The volume of dissolved hydrogen, V, in one completely reduced pellet at 1272 K is equal to 0.17 cm^3. It is assumed that, upon cooling, all the dissolved hydrogen diffuses out and fills the pores. Using the ideal gas law, the pressure of hydrogen in the pore volume at a temperature intermediate between the reduction temperature and ambient temperature (750 K) can be readily calculated. It is found to

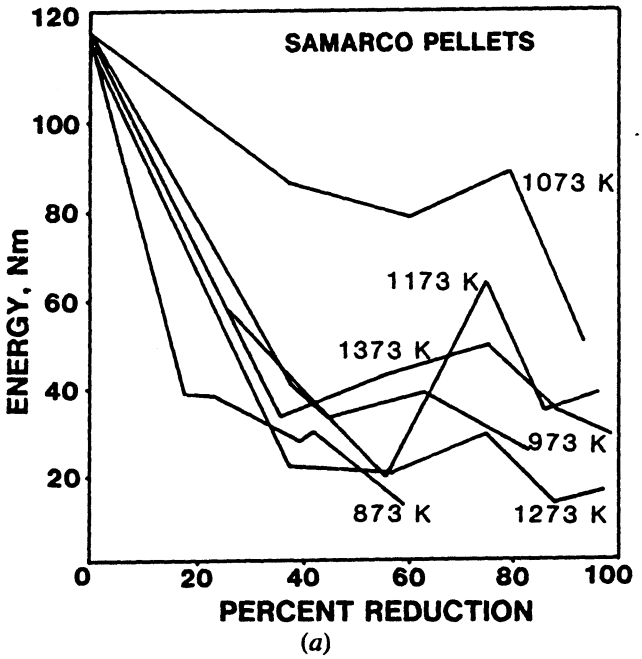

(a)

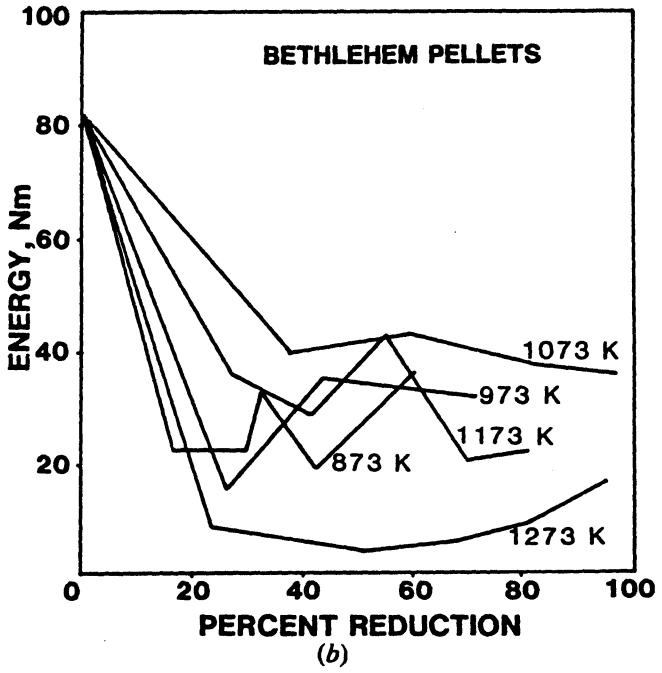

(b)

Fig. 7—(*a*) Energy required in the crushing process *vs* reduction for Samarco pellets. (*b*) Energy required in the crushing process *vs* percent reduction for Bethlehem pellets.

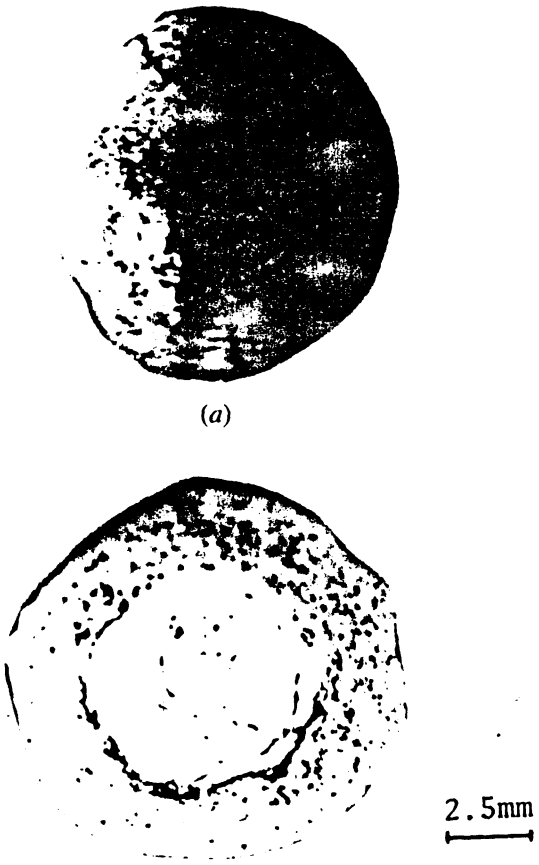

Fig. 8—Typical cracks observed in reduced pellets: (*a*) radial cracks, (*b*) circumferential cracks.

be equal to 2.92 atm, or 0.30 MN/m^2. This calculation is conservative, because the volume of pores is believed to increase with reduction, resulting in a decrease of P. When comparing this pressure to the ambient temperature compressive strength of the reduced pellets of this investigation (~3 MN/m^2), one can see that the internal pressure generated by trapped hydrogen is very low.

B. *Stress Analysis of Pellets during Reduction*

There are substantial volume changes associated with the structural changes in both the hematite-magnetite and magnetite-wustite transformation. Ottow,[19] as quoted by Meyer,[4] found a volume increase of 11 pct in the hematite-magnetite reaction. If one takes the specific gravities of hematite (6.85 g/cm^3) and magnetite (5.81 g/cm^3) and computes the density change by taking into account the loss in oxygen during the reaction, one arrives at a very close number: 9.8 pct volume increase. The calculations performed in this section assume a volume increase of 10 pct. For the wustite-iron phase transformation, one finds a contraction of 5 pct, incorporating the loss of oxygen during reaction into the calculation.

The analysis below applies to the hematite-magnetite reaction which (in a topochemical reaction) puts the hematite core under tension and the magnetite shell under compression. However, it can be extended to the other reaction involving a large volume change: the wustite-iron reaction, which has a volume change opposite in sign to the hematite-magnetite and magnetite-wustite reactions.

Consider a sphere that, prior to reduction, has a radius r_0 shown in Figure 9(a). After some reduction occurred, the sphere is composed of an unreduced core and a reduced shell. Consider the unreduced core separately as body 1, and the reduced shell as body 2; they have the dimensions shown in Figure 9(b), where r_i is radius of the core, r_i' is the inside radius of the shell, and r_o' is the outside radius of the

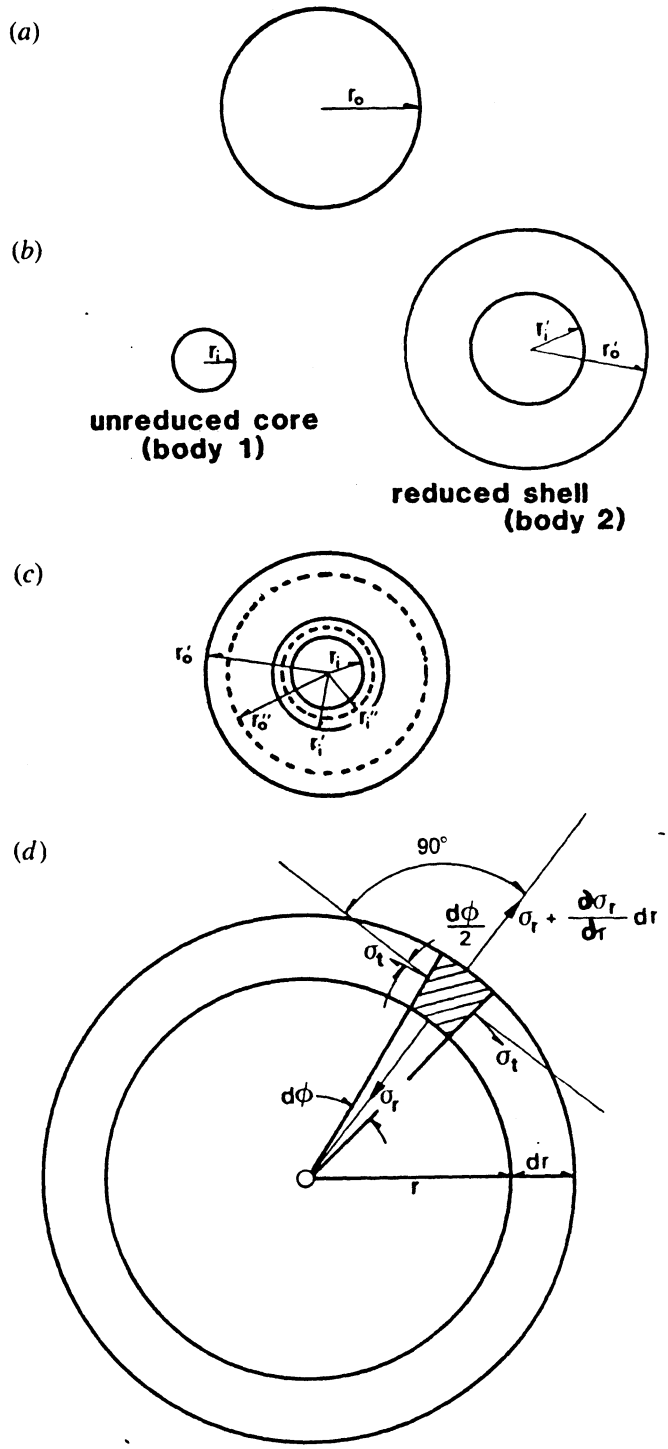

Fig. 9—Dimensional changes of pellets for stress analysis: (*a*) prior to reduction, (*b*) after reduction, (*c*) after binding, and (*d*) infinitesimal element for external shell.

shell. When reduction takes place, the increase in volume is defined as V/V_0. The relationship between r_i and r_i' is:

$$r_i' = \left(1 + \frac{\Delta V}{V_0}\right)^{1/3} r_i \qquad [1]$$

When bodies 1 and 2 are put together the final radius of the equilibrium interface (after binding) is r_i''. As seen in Figure 9(c), body 1 is expanded and body 2 is shrunk in order to reach equilibrium at r_i'' inside radius and r_o'' outside radius. The stress analysis will be conducted separately for the spherical core and for the shell. The boundary conditions will be applied in order to obtain the values of the interfacial stresses.

Unreduced Core (Body 1)

The bulk modulus B is the ratio between the hydrostatic pressure, σ_m or $-p$, and the dilatation Δ, that it produces[20]

$$B = \frac{\sigma_m}{\Delta} = \frac{1}{\beta} \qquad [2]$$

where β is the compressibility. Because the sphere is under hydrostatic stress, $\sigma_1 = \sigma_2 = \sigma_3$ and $\varepsilon_1 = \varepsilon_2 = \varepsilon_3$, which results in:

$$\sigma_m = \sigma_r = \sigma_t \qquad [3]$$

$$\Delta = 3\varepsilon_r = 3\varepsilon_t \qquad [4]$$

where σ_r and σ_t are the radial and tangential stresses, and ε_r and ε_t are the radial and tangential strains, respectively. For spherical coordinates the expression of ε_r in terms of displacement U can be written as (only radial displacements are assumed):

$$\varepsilon_r = \frac{\partial U}{\partial r} \qquad [5]$$

One can readily obtain

$$\frac{dU}{dr} = \frac{\sigma_r(1 - 2\nu)}{E} \qquad [6]$$

The solution of Eq. [6] can be obtained by integration:

$$U = \frac{\sigma_r(1 - 2\nu)r}{E} + C \qquad [7]$$

σ_r is constant because it is the stress at the interface, and C is the integration constant. When the radius of the core equals zero, $U = 0$; hence $C = 0$. The displacement of a point at the surface of the unreduced core is therefore described by:

$$U = \frac{\sigma_r(1 - 2\nu)r}{E} \qquad [8]$$

External Reduced Shell (Body 2)

Consider the static equilibrium of the element which is defined by two radii, r and $r + dr$, and an angle $d\phi$, as shown in Figure 9(d). This analysis is based on the one presented by Popov[21] for a thick-walled cylinder. The cylindrical coordinates were changed to spherical coordinates and the directions were modified accordingly. If the radial stress at the distance r is σ_r, the variable stress at the distance $r + dr$ will be $\sigma_r + d\sigma_r/dr\,dr$. The four tangential stresses acting on the other four faces of the element are σ_t. The corresponding forces are obtained by multiplying stresses by their respective areas. The area on which σ_r acts is $(r\,d\phi)^2$; that on which $\sigma_r + d\sigma_r/dr\,dr$ acts is $(r + dr)\,d\phi^2$; and each area on which σ_t acts is $r\,dr\,d\phi$. The weight of the element itself is neglected. Then, summing the forces along the radial direction, $\Sigma F_r = 0$,

$$\sigma_r(r\,d\phi)^2 - \left(\sigma_r + \frac{d\sigma_r}{dr}dr\right)^2 (r + dr)^2\,d\phi^2 + 4\sigma_t\frac{d\phi}{2}r\,dr\,d\phi = 0 \qquad [9]$$

Simplifying, and neglecting the infinitesimals of higher order, one obtains:

$$\frac{d\sigma_r}{dr} + \frac{2}{r}(\sigma_r - \sigma_t) = 0 \qquad [10]$$

This equation has two unknown stresses, σ_r and σ_t. To solve it, the geometry of deformation and properties of materials are used to express it in terms of one unknown displacement. The deformation of an element is described by its strain in the radial and tangential directions. If U represents the radial displacement of a surface of radius r, the strains ε_r and ε_t of an element in the radial and tangential directions are:

$$\varepsilon_r = \frac{\left(U + \frac{dU}{dr}\cdot dr\right) - U}{dr} = \frac{dU}{dr} \qquad [11]$$

$$\varepsilon_t = \frac{2\pi(r + U) - 2\pi r}{2\pi r} = \frac{U}{r} \qquad [12]$$

The stresses are related to strains by:

$$\varepsilon_r = \frac{1}{E}(\sigma_r - 2\nu\sigma_t) \qquad [13]$$

$$\varepsilon_t = \frac{1}{E}[-\nu\sigma_r + \sigma_t(1 - \nu)] \qquad [14]$$

Modifying Eqs. [13] and [14], one obtains:

$$\sigma_r = \frac{E}{(1 - 2\nu)(1 + \nu)}[(1 - \nu)\varepsilon_r + 2\nu\varepsilon_t] \qquad [15]$$

$$\sigma_t = \frac{E}{(1 - 2\nu)(1 + \nu)}(\nu\varepsilon_r + \varepsilon_t) \qquad [16]$$

Substituting ε_r and ε_t from Eqs. [11] and [12] into Eqs. [15] and [16], one finds

$$\sigma_r = \frac{E}{(1 - 2\nu)(1 + \nu)}\left[(1 - \nu)\frac{dU}{dr} + 2\nu\frac{U}{r}\right] \qquad [17]$$

$$\sigma_t = \frac{E}{(1 - 2\nu)(1 + \nu)}\left[\nu\frac{dU}{dr} + \frac{U}{r}\right] \qquad [18]$$

and, by substituting these values into Eq. [10] and simplifying, the desired differential equation is obtained:

$$r^2\frac{d^2U}{dr^2} + 2r\frac{dU}{dr} - \frac{2(1 - 2\nu)}{(1 - \nu)}U = 0 \qquad [19]$$

This differential equation with variable coefficients can be solved by making the substitution $U = r^n$. This leads to:

$$n^2 + n - \frac{2(1 - 2\nu)}{(1 - \nu)} = 0 \qquad [20]$$

This equation has the following roots:

$$m, n = -\frac{1}{2} \pm \sqrt{\frac{9 - 17\nu}{4(1 - \nu)}}$$

Since one has $\nu < 9/17$ for iron-ore pellets, the solution is:

$$U = A_1 r^n + A_2 r^m \qquad [21]$$

A_1 and A_2 are integration constants which must be determined from the conditions at the boundaries of the shell. Only one boundary condition is known: at $r = r_o$, $\sigma_{r_o} = 0$. Substituting Eq. [20] into Eq. [17], one obtains:

$$\sigma_r = \frac{E}{(1 - 2\nu)(1 + \nu)}\{A_1[(1 - \nu)nr^{(n-1)} + 2\nu r^{(n-1)}] + A_2[(1 - \nu)mr^{(m-1)} + 2\nu r^{(m-1)}]\} \qquad [22]$$

Applying the boundary condition to Eq. [22]:

$$A_2 = -\frac{(1 - \nu)nr_o^n + 2\nu r_o^n}{(1 - \nu)mr_o^m + 2\nu r_o^m} \quad A_1 = -BA_1 \qquad [23]$$

Parameter B was defined for convenience. Substituting A_1 from Eq. [22] into Eq. [21] and expressing it in terms of A_2:

$$A_2 = \frac{\sigma_r}{E} \frac{(1 - 2\nu)(1 + \nu)}{-\frac{1}{B}[(1 - \nu)nr^{(n-1)} + 2\nu r^{(n-1)}] + [(1 - \nu)mr^{(m-1)} + 2\nu r^{(m-1)}]} \qquad [24]$$

Substituting Eqs. [23] and [24] into Eq. [20], the final equation of the displacement of a general point inside the shell is:

$$U = \frac{\sigma_r(1 - 2\nu)(1 + \nu)}{E}\left\{\frac{r^n}{(1 - \nu)nr^{(n-1)} + 2\nu r^{(n-1)} - B[(1 - \nu)mr^{(m-1)} + 2\nu r^{(m-1)}]} + \frac{r^m}{-\frac{1}{B}[(1 - \nu)nr^{(n-1)} + 2\nu r^{(n-1)}] + [(1 - \nu)mr^{(m-1)} + 2\nu r^{(m-1)}]}\right\} \qquad [25]$$

C. *Binding of Internal Core with External Shell*

The displacement between bodies 1 and 2 can be determined from Eq. [1]. Since the core is under tension and the shell is under compression, minus signs are used to indicate compressive stresses. The sum of the displacements of the core (Eq. [8]) and of the shell (Eq. [25]) is equal to the radial displacement of the external shell, if it were isolated. This can be more clearly seen in Figure 9(c), where one can see that r_i has to expand to r_i'', and r_i' has to shrink to r_i'' in order to maintain the continuity at the boundary between the reduced and unreduced portions. This equality (Eq. [8] − Eq. [25] = Eq. [1] − r_i) leads to:

$$\sigma_r = \frac{E}{(1 - 2\nu)}\left[\left(1 + \frac{\Delta V}{V_0}\right)^{1/3} - 1\right] \cdot \left[\frac{1}{1 - \frac{1 + \nu}{(C - Br^{m-n}D)} - \frac{1 + \nu}{\left(\frac{-1}{B}r^{m-n}C + D\right)}}\right] \qquad [26]$$

where $C = (1 - \nu)n + 2\nu$ and $D = (1 - \nu)m + 2\nu$. Eq. [26] expresses the radial stress in terms of volume increase $\Delta V/V_0$, Poisson's ratio (ν), modulus of elasticity (E), and the initial radius of the pellet (r_o). An analogous procedure, utilizing Eq. [18] instead of Eq. [17], is used to obtain σ_t.

$$\sigma_t = \frac{E}{(1 - 2\nu)}\left[\left(1 + \frac{\Delta V}{V_0}\right)^{1/3} - 1\right] \cdot \frac{1}{\left[1 - \frac{1 + \nu}{F - B'Gr^{(m-n)}} - \frac{1 + \nu}{\frac{-1}{B}Fr^{(n-m)} + G}\right]} \qquad [27]$$

where $F = \nu n + 1$; $G = \nu m + 1$; and $B' = [(\nu n + 1)/(\nu m + 1)]r_o^{(n-m)}$. The calculation was made by using $\Delta V/V_0 = 0.10$ (this value is explained in the first part of Section IV), $r_o = 0.555$ cm, and $E = 3.14 \times 10^4$ MN/m (this is the E value for magnetite ore located at Mineville NY, which is lower than the E value for hematite ore located at Bessemer, AL, 6.69×10^4 MN/m^2 [22]). Figure 10(a) shows the variation of σ_r and σ_t generated at the interface with radius of interface for the hematite-magnetite transformation.

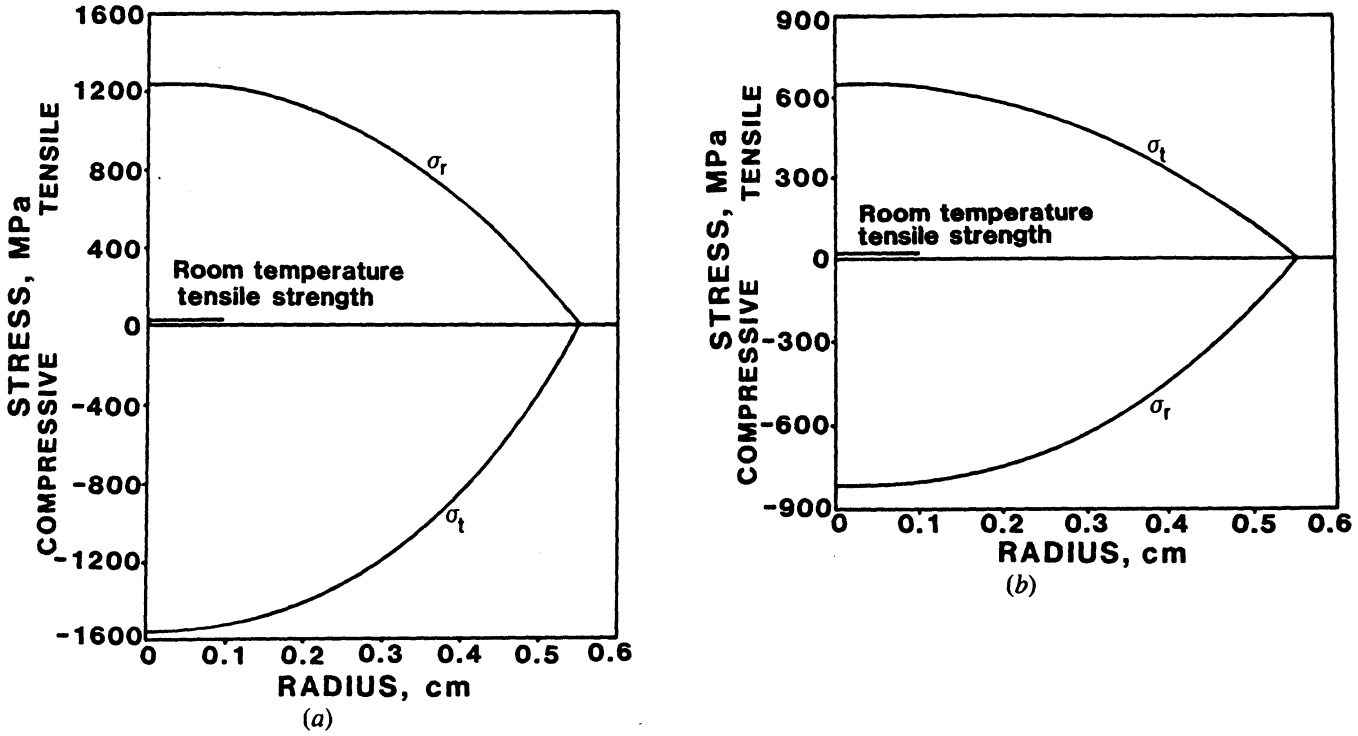

Fig. 10—Variation of radial (σ_r) and tangential (σ_t) stresses at reaction interface with pellet radius: (*a*) hematite-magnetite transformations; (*b*) wustite-iron transformation.

This analysis was applied to the wustite-iron reaction which puts the wustite core under compression and the iron shell under tension due to the decrease in volume; the change in volume is ~5 pct. The radial and tangential stresses can be expressed by Eqs. [26] and [27], by making $\Delta V/V_0 = -0.05$; the stresses are shown in Figure 10(b).

As seen from Figures 10(a) and 10(b), the smaller the radius of the interface (higher percent reduction), the higher the radial and tangential stresses generated for both reactions. For the hematite-magnetite reaction, the radial stress is tensile and the tangential stress is compressive. The wustite-iron reaction involves a volume change opposite in sign to the hematite-magnetite reaction, such that the radial and tangential stresses are opposite in sense to those of the hematite-magnetite reaction; this means the radial stress is compressive and the tangential stress is tensile. Minerals as well as ceramics exhibit a much higher resistance to compressive than to tensile stresses. Hence, the stresses of concern are σ_r for the hematite-magnetite reaction (Figure 10(a)) and σ_t for the wustite-iron reaction (Figure 10(b)). The tensile radial stresses will tend to produce the separation of the interface and cracks extending along it (circumferential cracks). The tensile tangential stresses will tend to produce cracks normal to their direction; these cracks will propagate along a radial plane. Hence, according to the stress analysis conducted above, the hematite-magnetite reaction will tend to produce circumferential cracks and the wustite-iron reaction will tend to produce radial cracks. The magnitude of the tensile stresses is amply sufficient to produce fracture. The tensile strength of the pellets (prior to reduction) at ambient temperature can be found from the crushing strength of the pellets. Hiramatsu and Oka,[23] Oka and Majima,[24] Jaeger,[25] and Meyers and Meyers[8] derived equations for the tensile stress in the interior of a sphere under uniaxial compression and arrived at the following equation for the tensile stress, σ, in the center of the sphere:

$$\sigma = k\frac{P}{r^2} \qquad [28]$$

where P is the compressive load, r is the pellet diameter, and k is a constant that is different for the different derivations but can be taken to be equal to 0.2. For a crushing strength of 2.5 kN (the average crushing strength of Samarco pellets) one obtains an equivalent tensile stress of 20 MN/m^2. This value is shown in Figures 10(a) and 10(b). It is evident that the tensile stresses generated by the reactions greatly exceed the tensile strength of the pellets.

V. CONCLUSIONS

1. The effect of reducing temperature on the mechanical strength of Samarco and Bethlehem Steel pellets was determined. The highest strength for both Samarco and Bethlehem Steel pellets was found to be after a reduction temperature of 1073 K which corresponds to low swelling or shrinking and relatively few small cracks exhibited by the pellets. Extensive swelling observed after reduction at higher temperatures resulted in a decrease of compressive strength.
2. Profuse cracking of the pellets was observed after most reduction experiments. Stress analysis showed that very high tensile radial and tangential stresses are generated at the interface of reduced regions, by volume changes involved in the hematite-magnetite and wustite-iron

transformations, respectively. These stresses are thought to be responsible for the radial and circumferential cracks observed.

ACKNOWLEDGMENTS

This research was supported by the New Mexico State Mining and Mineral Resources Research Institute, by the Royal Thai Government, and by the National Science Foundation (Grant DMR 8115127). Pellets used in this research were kindly provided by Mr. P. P. Meyers of Samarco Mineração (presently at Ferteco Mineração) and by Mr. Sudan Vidanage of Bethlehem Steel. The authors would like to acknowledge Mr. D. Baker, Dr. I. Gundiler, Mr. J. Reiche, Mr. E. Krosche, Dr. K. Oravecz, and Mr. S. Chang for valuable input to the work.

REFERENCES

1. E. T. Turkdogan: *Physical Chemistry of High Temperature Technology*, Academic Press, New York, NY, 1980, p. 303.
2. *Direct Reduced Iron: Technology and Economics of Production and Use*, R. L. Stephenson and R. M. Smailer, eds., Warrendale, PA, ISS-AIME, 1980.
3. E. T. Turkdogan and J. W. Vinters: *Can. Met. Quart.*, 1973, vol. 12, pp. 9-21.
4. K. Meyer: *Pelletizing of Iron Ores*, Springer-Verlag, Berlin, 1980, p. 167.
5. S. Taniguchi and M. Ohmi: *Trans. J.I.M.*, 1978, vol. 19, pp. 581-87.
6. S. Taniguchi and M. Ohmi: *Trans. J.I.M.*, 1980, vol. 12, pp. 433-40.
7. S. Taniguchi, M. Ohmi, and H. Fukuhara: *Trans. I.S.I. Jap.*, 1978, vol. 18, pp. 633-40.
8. M. A. Meyers and P. P. Meyers: *Trans. SME-AIME*, 1983, vol. 274, pp. 1875-84.
9. I.S.O. Technical Committee: "A Method for Determination of Crushing Strength," ISO/TC 102/SC 3 283E, February 1974.
10. W. M. Mckewan: *Trans. TMS-AIME*, 1958, vol. 212, pp. 791-93.
11. W. M. Mckewan: *Trans. TMS-AIME*, 1960, vol. 218, pp. 2-6.
12. E. T. Turkdogan and J. V. Vinters: *Metall. Trans.*, 1971, vol. 2, pp. 3174-96.
13. B. B. L. Seth and H. U. Ross: *Trans. TMS-AIME*, 1965, vol. 233, pp. 180-85.
14. J. Szekely, J. W. Evans, and H. Y. Sohn: *Gas-Solid Reactions*, Academic Press, New York, NY, 1976.
15. N. Towhidi and J. Szekely: *Ironmaking and Steelmaking*, 1981, pp. 237-49.
16. E. E. Hoffman, H. Rausch, W. Thumm, and E. Eisermann: *Stahl und Eisen*, 1970, vol. 90, pp. 676-82.
17. K. Meyer: *Pelletizing of Iron Ores*, Springer-Verlag, Berlin, 1980, p. 39.
18. *Metals Handbook*, 8th ed., Am. Soc. Met., 1973, vol. 8, p. 302, p. 973.
19. M. Ottow: Ph.D. Thesis, Tech. Un. Berlin, 1966.
20. G. E. Dieter: *Mechanical Metallurgy*, 2nd ed., McGraw-Hill, New York, NY, 1976, p. 18.
21. E. P. Popov: *Mechanics of Materials*, 2nd ed., Prentice Hall, Englewood Cliffs, NJ, 1976, p. 557.
22. R. S. Carmichael: *Handbook of Physical Properties of Rocks*, CRC Press, FL, 1982, vol. 2, p. 311.
23. Y. Hiramatsu and Y. Oka: *Intl. J. of Rock Mech. Min. Sci.*, 1966, vol. 3, pp. 89-99.
24. Y. Oka and M. Majima: *Can. Metall. Quart.*, 1970, vol. 9, p. 429.
25. J. C. Jaeger: *Intl. of Rock Mech.*, 1967, vol. 4, pp. 219-27.